PAPER

Check for updates

Investigation of BaO reinforced TiO_2–p_2O_5–li_2O glasses for optical and neutron shielding applications

Kh. S. Shaaban, [ID] *[a] Ateyyah M. Al-Baradi[b] and Atif Mossad Ali[cd]

The optical and radiation shielding characteristics of $15TiO_2$-$70P_2O_5$ – $(15 - x)$ Li_2O-x BaO $x = (0 \leq x \leq 10$ mol%) glasses were reported in this study. The glass status of the investigated samples was established by XRD. Although the molar volume decreases within 39.8–31.2 cm^3 mol^{-1}, the density was increased from 2.908 to 4.11 g cm^{-3} with the addition of BaO. UV-Vis-NIR spectroscopy was utilized for the examination of the optical characteristics of all compositions. $E_{opt.}^{indir}$ and $E_{opt.}^{dir}$ both increased from 2.7 to 3.07 eV and 2.79 to 3.31 eV, while E_u decreased from 0.368 to 0.295 eV. Furthermore, the Phy-X/PSD code was used to evaluate the gamma-ray shielding parameter. Within the energy range of 15 keV to 15 MeV, the equivalent atomic number, as well as the EBF and EABF parameters, was evaluated. Overall, excellent material properties were detected for a glass with a high BaO content, which could be useful for future optical, shielding, and fast neutron shielding properties.

1. Introduction

Glasses have unique characteristics like microhardness, optical, non-toxicity, and flexibility. The dominated incorporation of specialized transition metal oxides (TMO) into phosphate glasses allows them to be used in a variety of applications.[1–5] Adding various intermediate oxides to phosphate glasses has been found to improve their low chemical durability, according to several investigations. ZnO, CaO, BaO, ZrO_2, TiO_2, PbO_2, Bi_2O_3, Al_2O_3, and Fe_2O_3 are the most widely recommended additions to P_2O_5.[6–10]

Due to their unique physical characteristics, such as ultraviolet (UV) emission, excellent moisture resistance, and a high thermal expansion coefficient, TiO_2–P_2O_5 glasses have attracted a lot of attention in the last few decades. The main fields of application for TiO_2–P_2O_5 glasses are microelectronics, photonic materials, optical amplifiers, and semiconductors. Regrettably, binary TiO_2–P_2O_5 glass creation is limited, and elucidating these glasses requires a significant amount of energy. Glasses based on TiO_2–P_2O_5 have been studied as semiconductor materials for a long time. Furthermore, because Ti^{4+} has empty or unfilled d-shells, which can be attributed to polarizabilities, the presence of TiO_2 in P_2O_5 glasses may improve their optical and electrical characteristics. TiO_2–P_2O_5 based glasses have been considered as potential applicants for Raman applications because of all these distinctive optical characteristics.[3,7]

Alkaline oxides, in specific, are found to lower the melting temperature of TiO_2–P_2O_5 systems. When Li_2O is added to TiO_2–P_2O_5, lithium titanophosphate glasses are formed, which can be used in micro-batteries and electric devices. The optical absorption of glass systems is affected by the presence of TiO_2 and BaO. To minimize thermal expansion and enhance mechanically, and thermal stability, metal oxides such as BaO were added to the glass system.[11,12] BaO was doped in TiO_2–P_2O_5–Li_2O glasses in this investigation. Physical, optical, and radiation characteristics of BaO–TiO_2–P_2O_5–Li_2O glasses were developed and characterized.

The goal of this article was to develop BaO–TiO_2–P_2O_5–Li_2O glasses. This article can be used in the future for enhancing the optical requirements and to reduce the harmful effects of radiation on organisms. We have expanded our research into BaO in lithium titanophosphate glasses as a result of the above existing literature. As a result, we've developed lithium titanophosphate glasses with BaO substituted in a variety of compositions. In addition to the aforementioned studies, photons, neutrons, characteristics of BaO doped lithium titanophosphate glasses will be investigated using theoretical code in this work.

2. Materials and methods

The melt-quenching technique was utilized for manufacturing the glass system in Table 1 $70P_2O_5$–$15TiO_2$–$(15 - x)$ Li_2O − xBaO,

[a]*Department of Chemistry, Faculty of Science, Al-Azhar University, P. O. 71452, Assiut, Egypt. E-mail: khamies1078@yahoo.com*

[b]*Department of Physics, College of Science, Taif University, P. O. Box 11099, Taif, 21944, Saudi Arabia*

[c]*Physics Department, Faculty of Science, King Khalid University, Abha 61413, Saudi Arabia*

[d]*Department of Physics, Faculty of Science, Assiut University, Assiut, 71516, Egypt*

where $x = 0, 2, 4, 8$, and 10 mol%. A digital electronic balance was used to weigh starting materials such as titanium oxide, TiO_2, barium oxide BaO, lithium oxide Li_2O as Li_2CO_3, and phosphorous oxide P_2O_5 as $(NH_4)_2HPO_4$. The powder was put into the porcelain crucible and the mixture was preheated at 400 °C for 90 min. Then, the mixture was melted at 1150 °C. For the annealing procedure, the glasses were preheated at 375 °C to eliminate any thermal stress. The samples were cut to a thickness of 1 cm × 1 cm × 0.25 mm and polished on both sides before optical measurement. The UV-Vis-NIR data were collected at room temperature using a JASCO V-670 spectrometer. The absorption coefficient, (α), $\alpha = (2.303|d) \times A$, optical bandgap, $(E_{opt.}^{indir}$ & $E_{opt.}^{dir})$, Urbach energy, (E_u), refractive index (n_D), and dispersion parameters have been estimated using optical absorbance. Molar refractivity R_m, molar polarizability α_m, reflection loss R_L, metallization M, electronegativity χ, electron polarizability α, and optical basicity $\wedge$ were calculated as physical parameters related to optical energy:

$$R_m = V_m(1 - \sqrt{E_{opt.}/20}), \quad \alpha_m = \left(\frac{3}{4\pi N}\right)R_m. \quad R_L = \left(\frac{R_m}{V_m}\right).$$

$M = 1 - \dfrac{R_m}{V_m}$, $\chi = 0.2688E_{opt.}$ $\alpha = -0.9\chi + 3.5$ and $\wedge = -0.5\chi$

$+ 1.7$. R_m, α_m, $\alpha_0 2-$, and Λ were calculated as physical parameters related to the refractive index n_D: $R_m = n^2 - 1|n^2 + 2V_m$,

$$\alpha_m(3|4\pi N)R_m, \quad \alpha_0^{2-} = \frac{\left[\frac{V_m}{2.52}\left(\frac{n^2-1}{n^2+2}\right) - \sum \alpha_{cat}\right]}{N_o^{2-}}, \quad \text{and}$$

$$\Lambda = 1.67\left(1 - \frac{1}{\alpha_0^{2-}}\right).$$

Using the Archimedes Code, the density (ρ) of the investigated glasses is calculated. The following is the formula for calculating molar volume: $V_m = M/\rho$.

Ba_i content was determined $Ba_i = \left(\dfrac{6.023 \times 10^{23} \times \text{mol fraction of cation} \times \text{valency of cation}}{V_m}\right)$.

The inter-ionic, polaron, and internuclear distances were calculated as follows: $R_i = \left(\dfrac{1}{\text{concentration of Fe}_i}\right)^{\frac{1}{3}}$, $r_p = \dfrac{1}{2}\left(\dfrac{\pi}{6N}\right)^{\frac{1}{3}}$, and $r_i = \left(\dfrac{1}{N}\right)^{\frac{1}{3}}$. Ba–Ba separation is calculated using $(dBa - Ba) = \left(\dfrac{V_m^B}{N}\right)^{\frac{1}{3}}$ and $V_m^B = \dfrac{V_m}{2(1 - 2X_n)}$.

Phy-X/PSD is a new software developed by Sakar *et al.*[13] that can compute several shielding factors and parameters at any energies using a remote server with an Intel (R) Core(TM) i7-2600 CPU@3.40 GHz CPU and 1 GB installed memory.

Equivalent atomic number expected as $Z_{eq} = \dfrac{Z1(\log R2 - \log R) + Z2(\log R - \log R1)}{\log R2 - \log R1}$, the parameters for G–P fitting were calculated as follows: $P = \dfrac{P1(\log Z2 - \log Z_{eq}) + Z2(\log Z_{eq} - \log Z1)}{\log Z2 - \log Z1}$, P1 and P2 are G–P fitting variables that correlate to the atomic numbers Z1 and Z2. G–P fitting was used to estimate EABF and EBF.

$B(E,X) = 1 + \dfrac{b-1}{K-1}(K^x - 1)$ for $K \neq 1$, $B(E,X) = 1 + (b-1)x$ $K =$

1 where $K(E,X) = cx^a + d\dfrac{\tanh\left(\dfrac{x}{Xk} - 2\right) - \tanh(-2)}{1 - \tanh(-2)}$ for $x \leq 40$.

3. Results and discussion

3.1 Physical investigations

The XRD of the samples is depicted in Fig. 1, and they are all amorphous. The XRD showed a broad hump instead of peaks, demonstrating that the glasses are amorphous.[14–21]
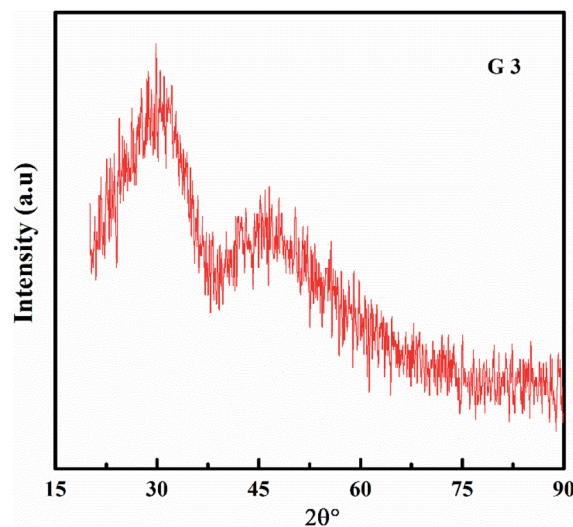

Fig. 1 XRD of $70P_2O_5–15TiO_2–11Li_2O–4BaO$ glasses.
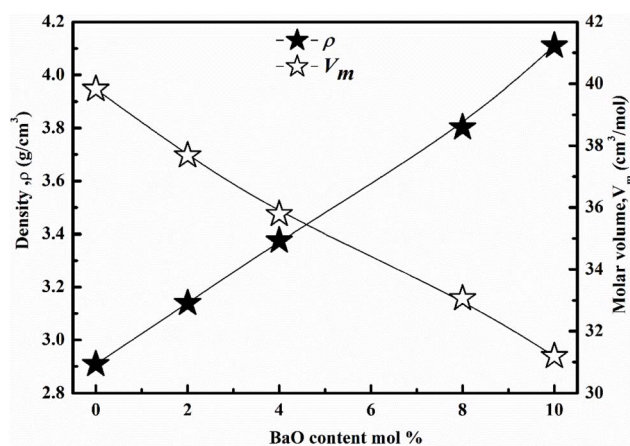
Fig. 2 Density & molar volume of glass system.

Table 1 Glasses that have been prepared have the following chemical composition

Code	P_2O_5	TiO_2	Li_2O	BaO
G 1	70	15	15	0
G 2	70	15	13	2
G 3	70	15	11	4
G 4	70	15	7	8
G 5	70	15	5	10

Table 2 Optical explanations of $15TiO_2$-$70P_2O_5$-$(15 - x)$ Li_2O-x BaO, glasses

Samples	G 1	G 2	G 3	G 4	G 5
N_O	3.95	3.95	3.95	3.95	3.95
$Ba_i \times 10^{21}$	—	0.64	1.35	2.92	3.87
(R_i)	—	11.79	9.20	7.11	6.48
(r_i)	—	13.61	10.64	8.25	7.52
(r_p)	—	3.91	3.06	2.37	2.16
dBa−Ba	0.58	0.56	0.55	0.53	0.51
R_m (cm^3 mol^{-1})	25.19	23.63	22.13	20.26	18.97
$\propto_m$ (A^3)	9.99	9.37	8.78	8.03	7.52
(R_L)	0.63	0.63	0.62	0.61	0.61
(M)	0.367	0.373	0.381	0.387	0.392
(χ)	0.73	0.75	0.78	0.81	0.83
(α°)	2.85	2.83	2.80	2.77	2.76
(Λ)	1.34	1.33	1.31	1.30	1.29
$E_{opt.}^{indir}$ (eV)	2.7	2.78	2.91	3	3.07
$E_{opt.}^{dir}$, (eV)	2.79	2.99	3.09	3.19	3.31
E_u (eV)	0.368	0.338	0.323	0.308	0.295
K_{th}	61.4	77.4	103.4	121.5	135.5
$T_{g(thero.)}$	387	419	472	508	536
V_i	0.7	0.74	0.778	0.847	0.9

Fig. 5 $(\alpha h\nu)^{1/2}$ against $(h\nu)$ to calculate $E_{opt.}^{indir}$.

As a function of BaO content, the density (ρ) and molar volume (V_m) are shown in Fig. 2. As the BaO content rises, (ρ) increment, but (V_m) decline. (ρ) values are affected by molecular weights and the density of oxide. Li_2O and BaO have densities (2.013 and 5.72 g cm^{-3}), as well as molecular weights (29.881 and 153.326).[22–25] A change in molar volume was shown to be the inverse of the density. Consequently, as packing density (V_i) rises, molar volume values decrease. The packing density (V_i) values are obtained in Table 2. As BaO replaces Li_2O, (V_m) decreases and (ρ) rises, resulting in a more compact glass structure.

The Ba^{2+} ion concentration increment as the (V_m decline. The, (R_i), (r_i), & (r_p) were predictable. These values decrease as Ba^{2+} increments. This trend was associated with a decrease in the (V_m).[25–27] Separation of Ba–Ba declines with Ba^{2+} increment, because of decrement in (V_m). The data values are obtained in Table 2.

3.2 Optical investigations

Fig. 3 shows the optical absorption data of glass samples at various BaO. (α), $E_{opt.}^{indir}$, $E_{opt.}^{dir}$, (E_U), & (n_D) have been estimated.
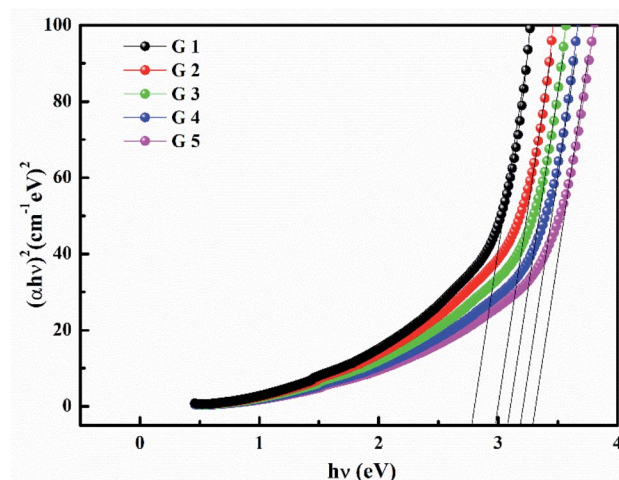

Fig. 3 Absorbance (A), transmittance (T), & reflectance (R) of glass system.
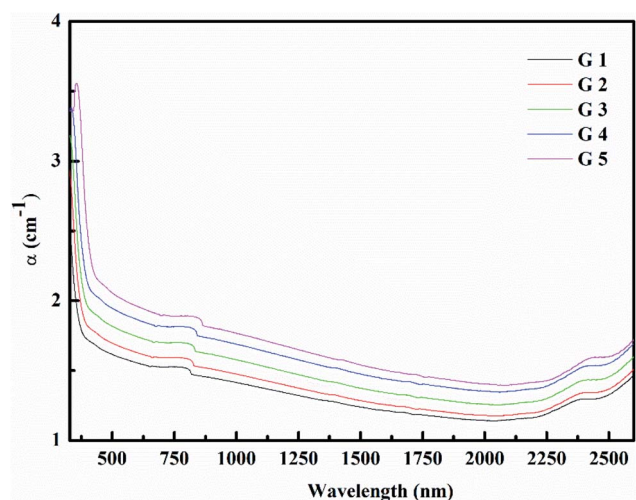
Fig. 4 Absorption coefficient of glass system.

Fig. 6 $(\alpha h\nu)^2$ against $(h\nu)$ to calculate $E_{opt.}^{dir}$.
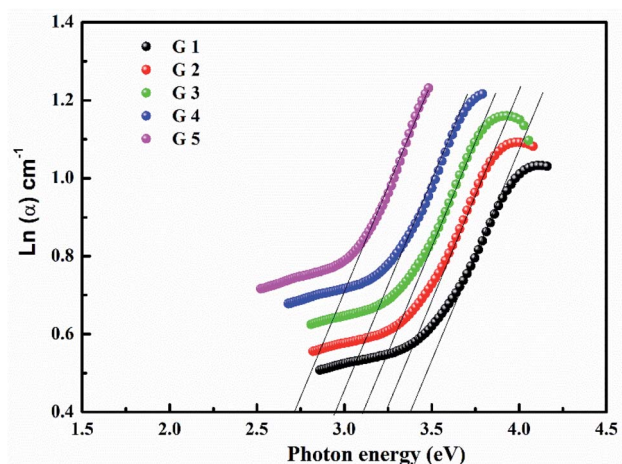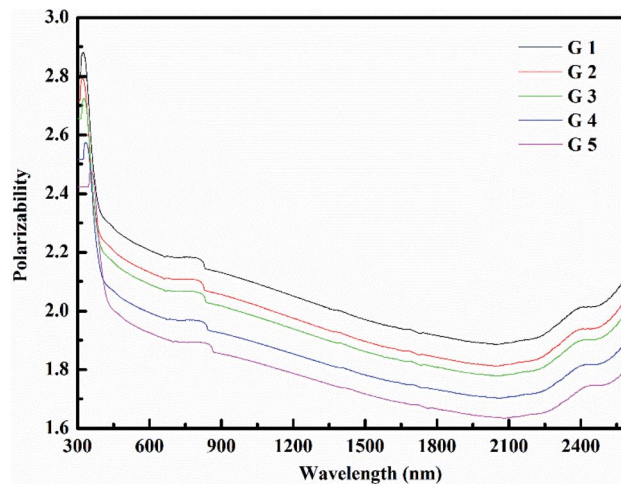
Fig. 7 $\ln(\alpha)$ against $(h\nu)$ to calculate E_u.
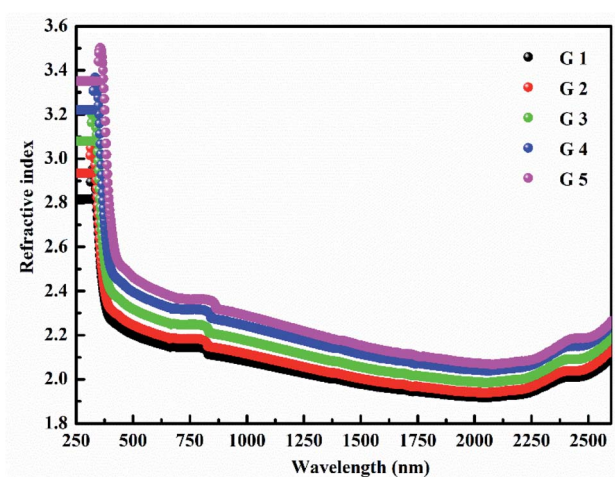

Fig. 10 polarizability of manufactured samples.

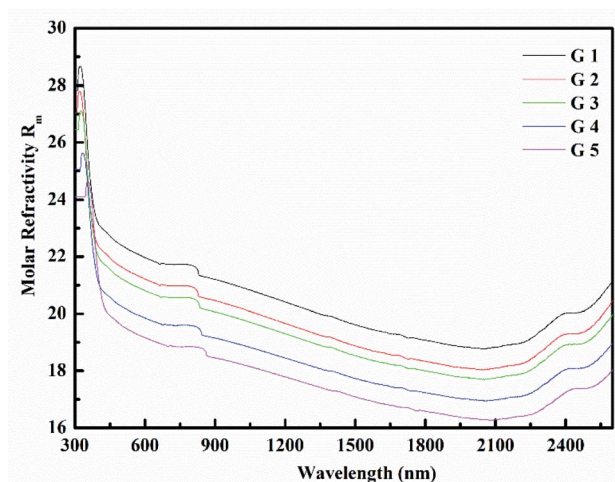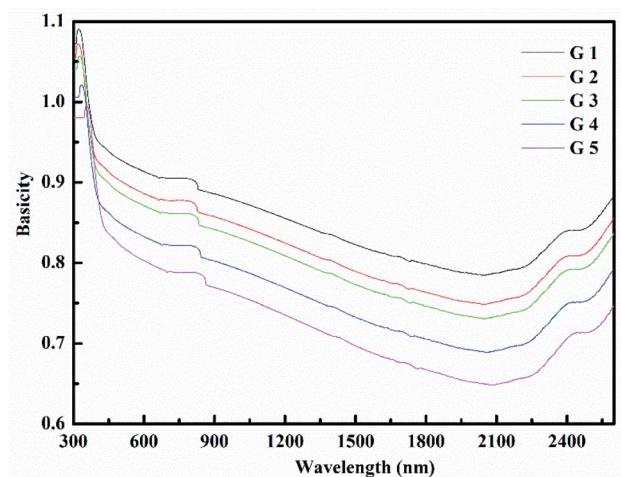
Fig. 8 Refractive index of manufactured samples.

(α) calculated as: $\alpha = (2.303|d) \times A$. ($\alpha$) of these samples are displayed in Fig. 4. Increase α to the increase in BaO concentration and light energy.[28–35]

Using the Tauc plot, $E_{opt.}^{indir}$ & $E_{opt.}^{dir}$ was determined as $\alpha h\nu = C(h\nu - E_{opt})^s$. Fig. 5 and 6 depict the correlation among both $(\alpha h\nu)^{1/2}$, $(\alpha h\nu)^2$, and $(h\nu)$. The intercepts were used to estimate $E_{opt.}^{indir}$ & $E_{opt.}^{dir}$ for the surveyed samples. $E_{opt.}^{indir}$ & $E_{opt.}^{dir}$ both increased in value as the BaO content raised. An increase in the bond length of the Ba (0.4347 nm) and Li (0.4347 nm) could explain this (0.3039 nm). The logarithm (α) is used to calculate (E_u) as a function of energy from the curve slope in Fig. 7. E_u decreases as BaO concentrations rise. As a function of BaO, the values of $E_{opt.}^{indir}$ n $E_{opt.}^{dir}$ & E_u are included in Table 1. Bulk module (K) and glass transition temperature ($T_{g(thero.)}$) are predictable in comparison to the optical bandgap $K_{th} = -478.93 + 200.13E_{opt.}$, $T_{g(thero.)} = -701.87 + 403.33E_{opt}$. K_{th} & $T_{g(thero.)}$ are increment as BaO, this is thought to be caused by an increase in the bandgap. The data values obtained are shown in Table 2.
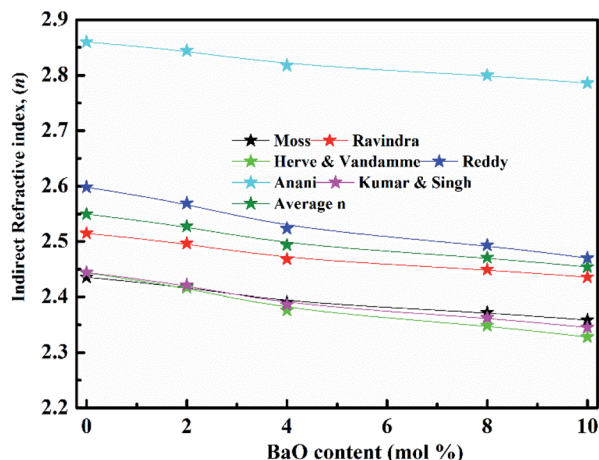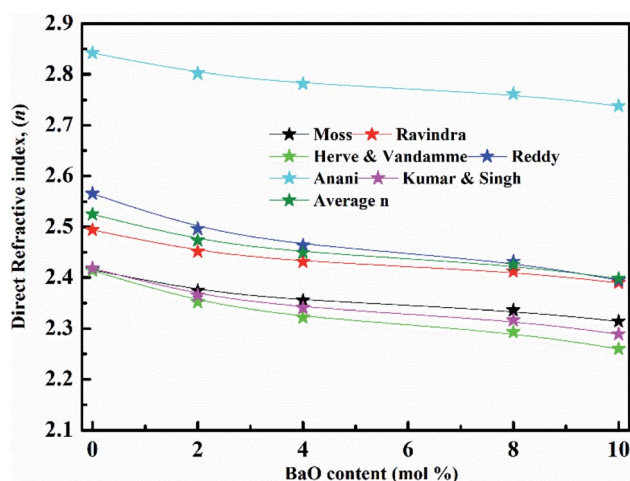

Fig. 9 Molar refractivity of manufactured samples.

Fig. 11 Basicity of manufactured samples.

RSC Advances

Paper

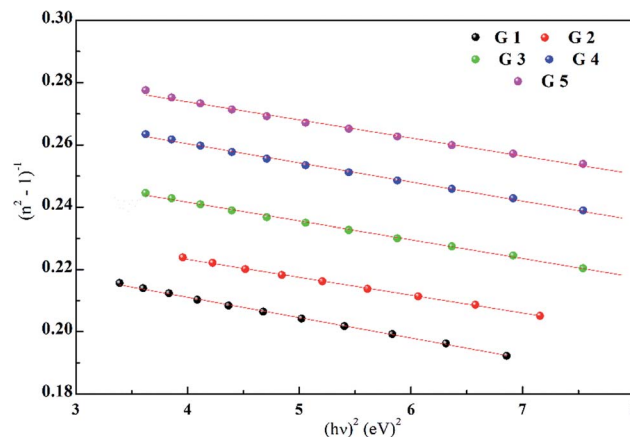Fig. 12 Non-linear refractive index for glasses.

Fig. 14 $(n^2 - 1)^{-1}$ with $(h\nu)^{-2}$ to calculate dispersion parameters.

Table 4 4Values of the dispersion parameters for the glass system

Code	G1	G2	G3	G4	G5
E_o	25.37	26.58	25.03	23.89	24.05
E_d	6.020	6.540	6.65	6.81	7.150
E_{opt}	3.01	3.27	3.324	3.400	3.573
n_o	1.10	1.12	1.125	1.13	1
ε_∞	1.24	1.25	1.27	1.285	1.297
S_o	1.952	2.064	2.078	2.079	2.084
λ	415	477	498	522	558

Fig. 13 Linear refractive index for glasses.

(n_D) was determined as $n_D = \dfrac{(1 - R)^2 + k^2}{(1 + R)^2 + k^2}$. As Fig. 8, the n_D of the investigated samples increment. n_D is increment as BaO, this is thought to be caused by an increase in density. n_D & ρ have a similar relationship.

R_m, $\propto_0^{2-}$ and (Λ) was estimated as n_D & exemplified in Fig. 9, 10, and 11. As the amount of BaO increases, these constructs deteriorate. This observation has been reduced due to the decrease in V_m.

According to $E_{opt.}^{indir}$, the values of (R_m), $(\propto_m)$, and (R_L) decrease, although (χ), M increment. This observation has been reduced due to the decrease in V_m. $\propto$ and $\wedge$ have different values of (χ), so they both decline. The data values obtained are shown in Table 2.

$E_{opt.}^{dir}$, and $E_{opt.}^{indir}$ are used to calculate the refractive index in Fig. 12 and 13. As an outcome, there is a minimal difference in the (n_D). The dielectric and static dielectric constants $(\varepsilon_o, \& \varepsilon_\infty)$ were estimated: $\varepsilon_o = -33.26876 + 78.61805 E_g - 45.70795 E_g 2 + 8.32449 E_g 3$, $\varepsilon_\infty = n_{AV}2$. Table 3 shows the effects of $E_{opt.}^{dir}$, and $E_{opt.}^{indir}$ on various optical constrictions.

Dispersion E_o and E_d were calculated as $n^2 - 1 = \dfrac{E_o E_d}{E_o^2 - E^2}$. E_o and E_d are calculated from the slope and intercept, as shown in Fig. 14 & Table 3. E_{opt} is the optical energy that represents $E_{opt} = \dfrac{E_d}{2}$. Refractive static index (n_o), oscillator's wavelength (λ_o), static dielectric ε_∞ and strength (S_o)
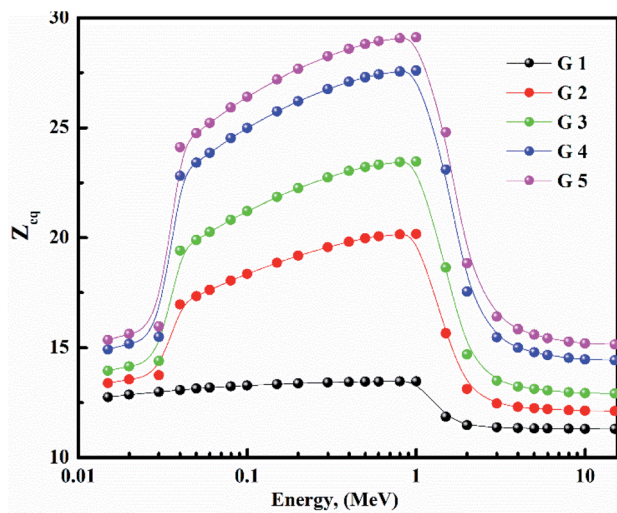
Table 3 The dielectric and static dielectric (ε_∞), (ε_o), Nonlinear parameter $\chi^{(1)}$, $(\chi^{(3)})$ and average refractive index (n_2) value as a function of $E_{opt.}^{indir}$.

Sample name	ε_∞	ε_0	$\chi^{(1)}$	$(\chi^{(3)})$ 10^{-12} (esu)	(n_2) 10^{-11} (esu)
G 1	6.45	9.64	0.438	6.25	9.24
G 2	6.39	10.89	0.4297	5.76	8.59
G 3	6.22	13.58	0.4155	5.07	7.66
G 4	6.11	15.97	0.4059	4.64	7.08
G 5	6.02	18.16	0.4	4.34	6.6
Value as a function of $E_{opt.}^{dir}$.					
G 1	6.376	11.1	0.428	5.71	8.5
G 2	6.12	15.68	0.407	4.69	7.14
G 3	5.998	18.84	0.398	4.26	6.56
G 4	5.88	22.62	0.389	3.88	6.03
G 5	5.75	28.06	0.378	3.47	5.46

Fig. 15 Equivalent atomic number for glasses.

3.3 Radiation attenuation capacities

Fig. 15 depicts the Z_{eq} results graphically. When the incident photon energy was increased and Li_2O was replaced with BaO, the (Z_{eq}) enhanced then decreased. Due to the photoelectric process, the Z_{eq} is smallest at low energy, then suddenly increases in the middle energy region due to Compton scattering, and finally, the Z_{eq} is reduced due to the pair production process. Because of the pair creation interaction, the (Z_{eq}) value decreases at energies higher than 1 MeV.[36-45] As a result, glass with a higher BaO content has a higher Z_{eq} than others. In all photon energy, it was discovered that G 5 has the maximum values, while G 1 has the smallest.

Using the (G-P) fitting method, the (EBF) and (EABF) were calculated. Fig. 16 show EBF and EABF. The pattern of variation for both EAF & EABF is similar. Because of the different dominant interaction processes, the EBF and EABF rise, and decline. One common feature of the EAF & EABF spectra is that the Compton scattering (CS) dominated areas have relatively higher values when compared to both photoelectric effect (PE) and pair production (PP). This also confirms that a material's EAF & EABF is determined by its photon energy and chemical structure. In addition, as BaO content increases, the EAF & EABF decrease. As a result, the EBF and EABF variance behaviors are primarily impacted by the three main interaction mechanisms discussed previously.[38-45]

was expected as $n_0 = \sqrt{1 + \frac{E_d}{E_0}}$, $\varepsilon_\infty = n_0 2$, (λ_o) & (S_o) & $n^2 - 1 = \frac{S_0 \lambda_0^2}{1 - \left(\frac{\lambda_0}{\lambda}\right)2}$. The items available are listed in Table 4.
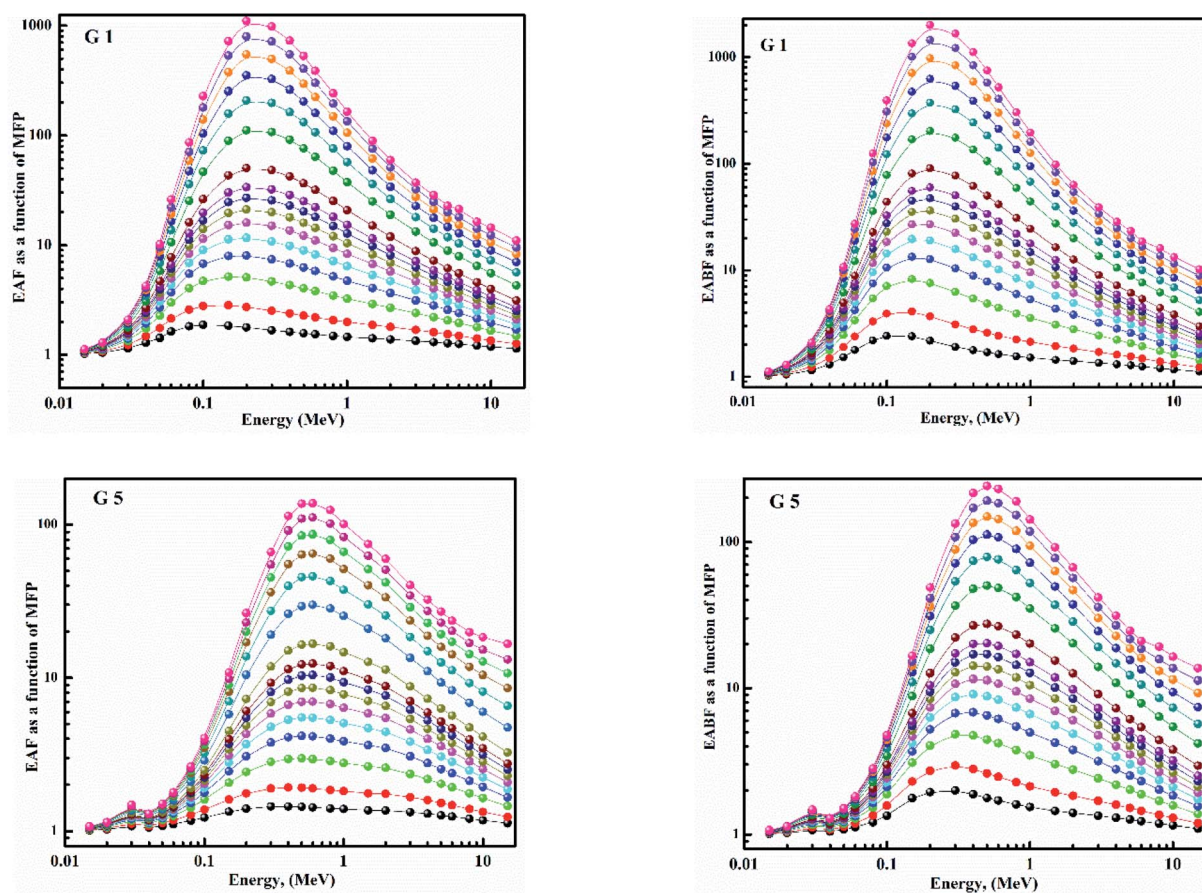
Fig. 16 EAF & EABF for $70P_2O_5-15TiO_2-15Li_2O$ & $70P_2O_5-15TiO_2-5Li_2O-10BaO$ glasses.
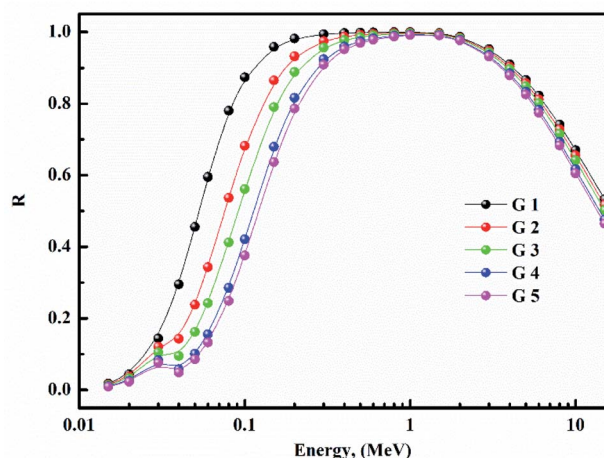
Fig. 17 Effective removal cross-sections for fabricated glasses.

Finally, we investigate the neutron shielding behavior of glasses using effective removal cross-sections $\sum R$. $\sum R$ of synthesized samples is shown in Fig. 17. $\sum R$ is a density-dependent is shown in Fig. 18a and b. Clearly, as the BaO
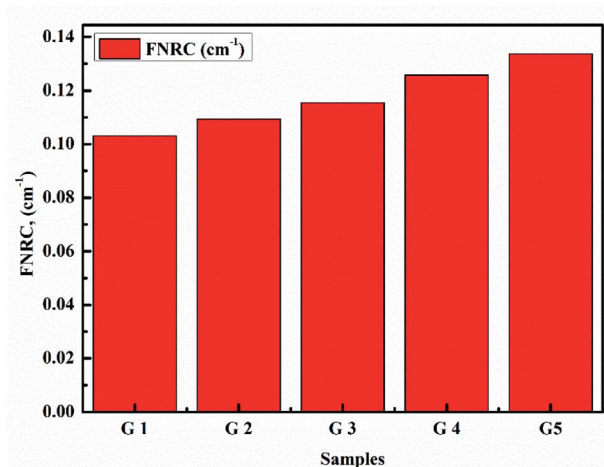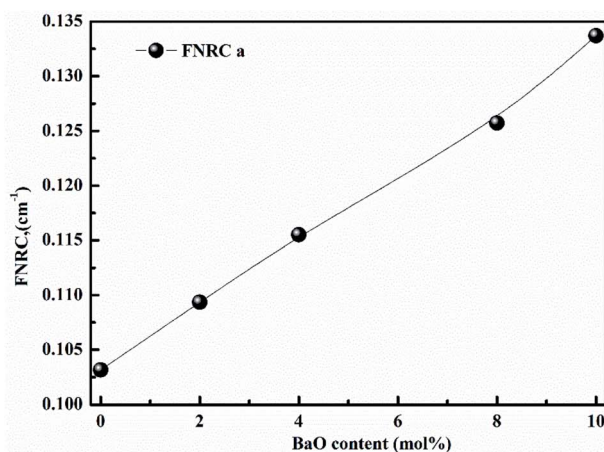
content of the glasses increases, $\sum R$ increases. When the FNRC of glass samples is compared, G 5 is a better fast neutron absorber. As a result, the highest value is given to G 5. The glass sample G 5 is the best choice for neutron attenuation applications.[38–45]

4. Conclusions

Melt quenching performance was utilized to manufacture lithium titanophosphate glasses doped with different amounts of BaO for optics and radiation applications. The XRD analysis confirmed the amorphous state. The molar volume is the decline within 39.8–31.2 cm³ mol⁻¹, the density was increment from 2.908 to 4.11 g cm⁻³ with an increase of BaO. With increment BaO, the studied glasses' linear and nonlinear optical properties improve significantly. $E_{opt.}^{indir}$ & $E_{opt.}^{dir}$ both increased from 2.7 to 3.07 eV, 2.79 to 3.31 eV, while E_u decline from 0.368 to 0.295 eV. For all glasses, the metallization ranged from 0.367 to 0.392, and electronegativity ranged from 0.73 to 0.83. The (EBF and EABF) values reduced slightly as the BaO increased. Overall, excellent material properties were detected, which could be useful for future optical applications. Consequently, these glasses can be suggested and improved as shielding material for gamma-ray & neutrons.

Conflicts of interest

There are no conflicts to declare.

Acknowledgements

References

1 J. Šubčík, L. Koudelka, P. Mošner, L. Montagne, B. Revel and I. Gregora, *J. Non-Cryst. Solids*, 2009, **355**, 970–975.

2 A. A. El-Maaref, R. M. El-Agmy, K. S. Shaaban and E. A. Abdel Wahab, *Eur. Phys. J. Plus*, 2021, **136**, 804.

3 M. A. Sayed, A. M. Ali, A. F. Abd El-Rehim, E. A. Abdel Wahab and K. S. Shaaban, *J. Elec. Mat.*, 2021, **50**, 3116–3128.

4 K. S. Shaaban, E. A. Abdel Wahab, A. A. El-Maaref, M. Abdelawwad, E. R. Shaaban, E. S. Yousef, H. Wilke, H. Hillmer and J. Börcsök, *J. Electron. Mater.*, 2020, **31**, 4986–4996.

5 A. A. El-Maaref, S. Badr, K. S. Shaaban, E. A. Abdel Wahab and M. M. Elokr, *J. Rare Earths*, 2019, **37**, 253–259.

6 E. A. Abdel Wahab, A. A. El-Maaref, K. S. Shaaban, J. Börcsök and M. Abdelawwad, *Opt. Mat.*, 2021, **111**, 110638.

7 K. S. Shaaban, E. S. Yousef, S. A. Mahmoud, E. A. A. Wahab and E. R. Shaaban, *J. Inorg. Organomet. Polym. Mater.*, 2020, **30**, 4655–4663.

Fig. 18 (a) Fast neutron removal cross-sections with BaO. (b) Fast neutron removal cross-sections with samples.

8 K. S. Shaaban, H. Y. Zahran, I. S. Yahia, H. I. Elsaeedy, E. R. Shaaban, S. A. Makhlouf, E. A. A. Wahab and E. S. Yousef, *Appl. Phys. A: Solids Surf.*, 2020, 126.

9 Y. S. Rammah, F. I. El-Agawany, E. A. A. Wahab, M. M. Hessien and K. Shaaban, *Radiat. Phys. Chem.*, 2022, 109956, DOI: 10.1016/j.radphyschem.2021.109956.

10 Z. A. Alrowaili, A. M. Ali, A. M. Al-Baradi, M. S. Al-Buriahi, E. A. A. Wahab and K. S. Shaaban, *Opt. Quantum Electron.*, 2022, **54**, 88–106.

11 A. F. A. El-Rehim and K. S. Shaaban, *J. Mater. Sci.: Mater. Electron.*, 2021, **32**, 4651–4671.

12 K. S. Shaaban, S. Alomairy and M. S. Al-Buriahi, *J. Mater. Sci.: Mater. Electron.*, 2021, **32**, 26034–26048.

13 E. Şakar, Ö. F. Özpolat, B. Alım, M. I. Sayyed and M. Kurudirek, *Radiat. Phys. Chem.*, 2020, **166**, 108496.

14 K. H. Mahmoud, A. S. Alsubaie, E. A. A. Wahab, F. M. Abdel-Rahim and K. S. Shaaban, *Silicon*, 2021, DOI: 10.1007/s12633-021-01125-0.

15 K. S. Shaaban and E. S. Yousef, *Optik*, 2020, **203**, 163976.

16 K. S. Shaaban, I. Boukhris, I. Kebaili and M. S. Al-Buriahi, *Silicon*, 2021, DOI: 10.1007/s12633-021-01080-w.

17 A. F. A. El-Rehim, H. Y. Zahran, I. S. Yahia, A. M. Ali and K. S. Shaaban, *Silicon*, 2020, DOI: 10.1007/s12633-020-00827-1.

18 A. F. A. El-Rehim, A. M. Ali, H. Y. Zahran, I. S. Yahia and K. S. Shaaban, *J. Inorg. Organomet. Polym. Mater.*, 2021, **31**, 1774–1786.

19 K. S. Shaaban and Y. B. Saddeek, *Silicon*, 2017, **9**, 785–793.

20 A. F. A. El-Rehim, K. S. Shaaban, H. Y. Zahran, I. S. Yahia, A. M. Ali, M. M. A. Halaka, S. A. Makhlouf, E. A. A. Wahab and E. R. Shaaban, *J. Inorg. Organomet. Polym. Mater.*, 2021, **31**, 1057–1065.

21 B. Albarzan, A. H. Almuqrin, M. S. Koubisy, E. A. Abdel Wahab, K. A. Mahmoud, Kh. S. Shaaban and M. I. Sayyed, *Prog. Nucl. Energy*, 2021, **141**, 103931.

22 A. F. A. El-Rehim, K. S. Shaaban, H. Y. Zahran, E. A. A. Wahab and E. R. J. Shaaban, *Mat. Sci. Mat. In Elec.*, 2021, **31**(3), 1057–1065. https://www.scopus.com/sourceid/4700152855?origin=resultslist.

23 K. S. Shaaban, A. M. Al-Baradi and E. A. A. Wahab, *Silicon*, 2021, DOI: 10.1007/s12633-021-01309-8; E. A. A. Wahab, A. M. Al-Baradi, M. A. Sayed, A. M. Ali, S. A. Makhlouf and K. S. Shaaban, *Silicon*, 2022, DOI: 10.1007/s12633-021-01652-w.

24 E. A. Abdel Wahab, A. A. El-Maaref, K. S. Shaaban, J. Börcsök and M. Abdelawwad, *Opt. Mat.*, 2021, **111**, 110638.

25 A. A. El-Maaref, E. A. A. Wahab, K. S. Shaaban and R. M. El-Agmy, *Solid State Sci.*, 2021, **113**, 106539.

26 A. M. Al-Baradi, E. A. A. Wahab and K. S. Shaaban, *Silicon*, 2021, DOI: 10.1007/s12633-021-01286-y.

27 A. M. Al-Baradi, A. F. A. El-Rehim, Z. A. Alrowaili, M. S. Al-Buriahi and K. S. Shaaban, *Silicon*, 2021, DOI: 10.1007/s12633-021-01481-x.

28 M. S. I. Koubisy, K. S. Shaaban, E. A. A. Wahab, M. I. Sayyed and K. A. Mahmoud, *Eur. Phys. J. Plus*, 2021, **136**(2), 156.

29 E. A. A. Wahab, A. M. Aboraia, A. M. E. Shafey, K. S. Shaaban and A. V. Soldatov, *Opt. Quantum Electron.*, 2021, **53**, 504.

30 E. A. Abdel Wahab, K. S. Shaaban, S. Alomairy and M. S. Al-Buriahi, *Eur. Phys. J. Plus*, 2021, **136**, 636.

31 E. A. Abdel Wahab, K. S. Shaaban and E. S. Yousef, *Opt. Quantum Electron.*, 2020, **458**, 52.

32 S. Alomairy, A. M. Aboraia, E. R. Shaaban and K. S. Shaaban, *Braz. J. Phys.*, 2021, **51**, 1237–1248.

33 E. A. A. Wahab, K. S. Shaaban and A. M. Al-Baradi, *Silicon*, 2021, DOI: 10.1007/s12633-021-01236-8.

34 A. M. Fayad, K. S. Shaaban, W. M. Abd-Allah and M. Ouis, *J. Inorg. Organomet. Polym. Mater.*, 2020, **30**, 5042–5052.

35 Z. A. Alrowaili, A. M. Al-Baradi, M. A. Sayed, A. Mossad Ali, E. A. Abdel Wahab, M. S. Al-Buriahi and K. S. Shaaban, *Optik*, 2022, **249**, 168259.

36 A. M. Ali, Z. A. Alrowaili, A. M. Al-Baradi, M. S. Al-Buriahi, E. A. A. Wahab and K. S. Shaaban, *Silicon*, 2021, DOI: 10.1007/s12633-021-01440-6.

37 E. A. Abdel Wahab and K. S. Shaaban, *Appl. Phys. A*, 2021, **127**(12), 956.

38 K. S. Shaaban, H. Y. Zahran, I. S. Yahia, H. I. Elsaeedy, E. R. Shaaban, S. A. Makhlouf, E. A. A. Wahab and E. S. Yousef, *Appl. Phys. A*, 2020, **126**(10), 804.

39 M. A. Alothman, Z. A. Alrowaili, J. S. Alzahrani, E. A. A. Wahab, I. O. Olarinoye, C. Sriwunkum, K. S. Shaaban and M. S. Al-Buriahi, *J. Alloys Compd.*, 2021, **882**, 160625.

40 A. F. A. El-Rehim, H. Y. Zahran, I. S. Yahia, E. A. A. Wahab and K. S. Shaaban, *J. Mater. Eng. Perform.*, 2021, **30**, 1872–1884.

41 A. F. A. El-Rehim, H. Y. Zahran, I. S. Yahia, S. A. Makhlouf and K. S. Shaaban, *Silicon*, 2021, **13**, 2289–2307.

42 Y. B. Saddeek, K. H. S. Shaaban, R. Elsaman, A. El-Taher and T. Z. Amer, *Radiat. Phys. Chem.*, 2018, **150**, 182–188.

43 S. Alomairy, Z. A. Alrowaili, I. Kebaili, E. A. A. Wahab, C. Mutuwong, M. S. Al-Buriahi and K. S. Shaaban, *Silicon*, 2021, DOI: 10.1007/s12633-021-01347-2.

44 S. Alomairy, M. S. Al-Buriahi, E. A. Abdel Wahab, C. Sriwunkum and K. Shaaban, *Ceram. Interfaces*, 2021, **47**(12), 17322–17330.

45 M. H. A. Mhareb, M. I. Sayyed, Y. S. M. Alajerami, M. Alqahtani, N. Dwaikat, A. M. Alsagry, M. Al-Yatimi and M. Zakariah, *Eur. Phys. J. Plus*, 2021, **136**, 26–41.